The Glass-to-Glass Transition and Its End Point in a Copolymer Micellar System

Sow-Hsin Chen,[1]* Wei-Ren Chen,[1] Francesco Mallamace[2]

We present experimental evidence, obtained from small-angle neutron scattering and photon correlation measurements, indicating the existence of two types of structurally arrested (glassy) states in a copolymer micellar system with a short-range interparticle attractive interaction. Within a certain range of micellar volume fractions, a sharp transition between these two types of glass is observed by varying the temperature. Furthermore, we found an end point of this transition line beyond which the two glasses become identical in their local structure and their long-time dynamics. These findings confirm the recent mode-coupling theory predictions regarding the phase behavior of the structurally arrested states for this type of system.

The study of the kinetic glass transition, or structural arrest transition in systems with short-range attraction, has attracted increasing attention lately because investigations of it may lead to the understanding of the so-far ill-characterized gelation states that are commonly observed in soft matter such as colloidal systems and protein solutions (*1*). Mode-coupling theory (MCT) gives a fairly accurate description of the dynamic slowing-down process near the transition from a supercooled liquid to a solid-like amorphous (glassy) state (*2, 3*). Many colloidal systems can be modeled as spherical particles interacting via a specific form of pairwise effective potential. We can thus conveniently test the validity of MCT by comparing experimental results obtained from a colloidal system with results calculated explicitly with the use of a specific interparticle potential. Initially, a hard-sphere system with a purely repulsive interaction potential was used to model the colloidal system. In this case at low volume fractions, the behavior of the colloidal system is fluid-like. As the volume fraction increases, the particles exhibit a two-stage relaxation process. The initial decay corresponds to the rattling of a typical particle confined within a transient cage formed by its neighbors and is followed by a slow decay resulting from relaxation of the cage itself and the escape of the trapped particle. The latter process leads to a possibility of particle diffusion through the structural relaxation. At a critical volume fraction ϕ_c, which was predicted to be 0.516 but determined experimentally to be 0.58 (*4*), both the particle diffusion and the long-time density fluctuations freeze, and the system undergoes an ergodic-to-nonergodic transition, which is defined as the kinetic glass transition in the literature (*2, 3*). Although this prediction has been substantiated with the use of dynamic light scattering (*4–6*), confocal microscopy (*7, 8*), and computer simulations (*9*), there are still some anomalous dynamical observations that cannot be interpreted in terms of the hard-sphere potential (*10, 11*). Recent MCT calculations with more accurate descriptions of the particle interactions (*12–16*) show that if the system is characterized by a hard core plus an additional short-range attractive interaction (an adhesive hard-sphere system, AHS), a different dynamical arrest scenario emerges. In an AHS, a second external control parameter, temperature, is introduced into the description of the phase behavior in addition to the volume fraction, and loss of ergodicity can take place by either increasing the volume fraction or changing the temperature. It is thus possible for the system to undergo a reentrant liquid-to-glass transition. At high temperatures and at sufficiently high volume fractions, the system evolves into the well-known glassy state called a repulsive glass. However, at relatively low temperatures, an attractive glass can form where the particle motion is hindered by cluster formation with neighboring particles. In an AHS, aside from the hard-core diameter, an additional length scale, the range of the attractive well, should come into play. With this insight, we may divide spherical colloidal systems into two categories: the one–length scale hard-sphere system, in which the glass formation is dictated by the cage effect, and the two–length scale AHS, in which the two glass-forming mechanisms may coexist and compete with each other. Furthermore, MCT shows that in an AHS with sufficiently small ratios of the range of the attractive interaction to the hard-core diameter, variation of the control parameters allows the transition be-

[1]Department of Nuclear Engineering, Massachusetts Institute of Technology (MIT), Cambridge, MA 02139, USA. [2]Dipartmento di Fisca e Instituto Nazionale per la Fisica della Materia, Universita' di Messina, I-98100 Messina, Italy.

*To whom correspondence should be addressed. E-mail: sowhsin@mit.edu
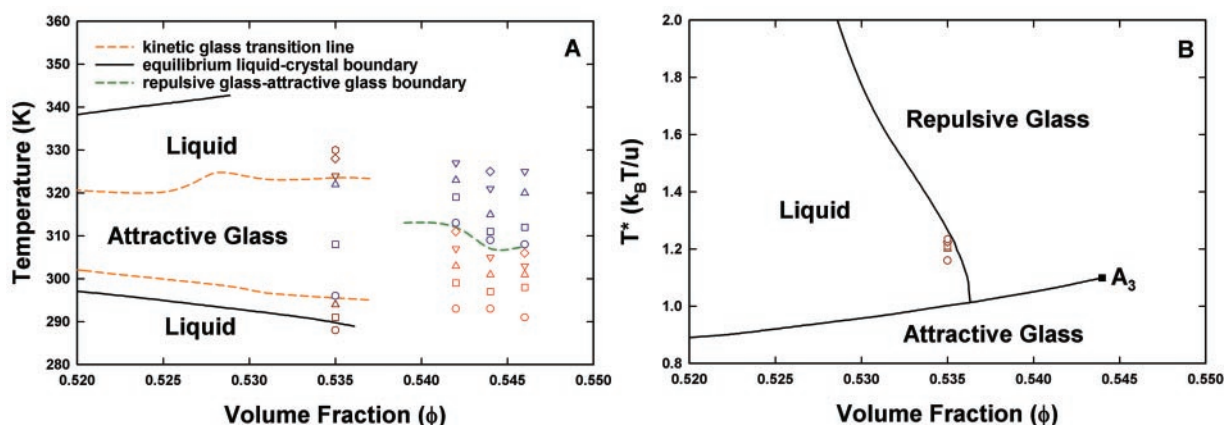
Fig. 1. The experimental phase diagram of the L64/D_2O micellar system (**A**) compared with the theoretical phase diagram predicted by MCT calculations for the case of $\varepsilon = 0.03$ (**B**). At $\phi = 0.535$, the phase points in the liquid regions shown in (A) can be mapped into the corresponding liquid region in the theoretical phase diagram in (B) with the use of the results of SANS data analyses. The symbols in (A) at the three higher volume fractions (glass region) indicate the phase points where the experimental data are taken and shown in Fig. 2, B to D.

tween these two distinct forms of glass (see Fig. 1B for the predicted phase diagram). Of particular interest is the occurrence of an A_3 singularity at which point the glass-to-glass transition line terminates. MCT suggests that the two distinct dynamically arrested states become identical at and beyond this point.

Several ongoing experimental investigations have confirmed some of the theoretical predictions, such as the reentrant glass transition phenomenon and the logarithmic relaxation of the glassy dynamics. They are considered to be signatures of the glassy dynamics in the two–length scale system (17–21). Yet except for a recent report on its realization in a dense micellar system (22), a detailed investigation of the glass-to-glass transition, although not uncommon in pure substances (23), remains incomplete, and the physical insight into the slow dynamics near its associated A_3 singularity is still lacking.
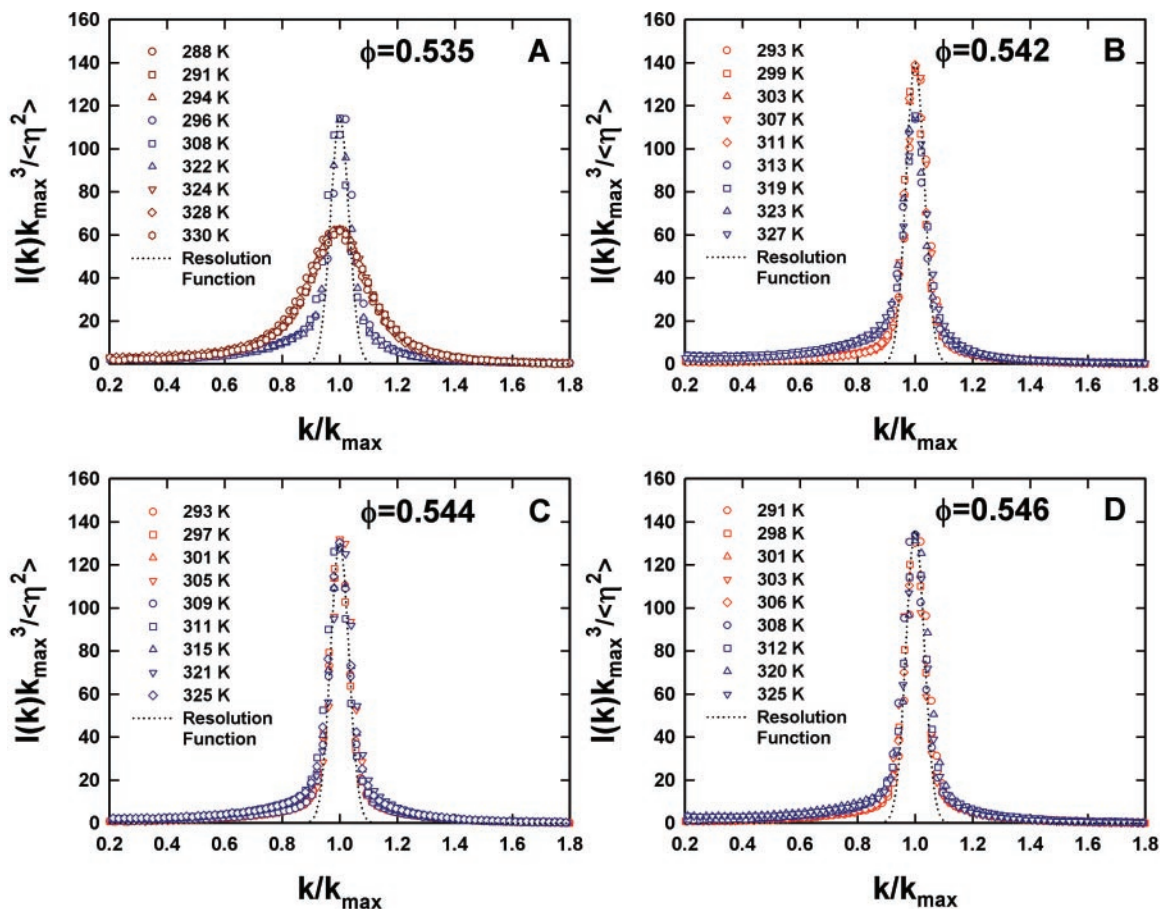
We present a detailed study of the glass-to-glass transition in a dense micellar system, focusing on the local structure and dynamics of the system near the A_3 singularity. Our micellar system was made by dissolving a triblock copolymer L64, one member of Pluronic (BASF AG, Ludwigshafen, Germany) family, used extensively in industrial applications, into D_2O at different weight fractions C. Pluronic is made of polyethylene oxide (PEO) and polypropylene oxide (PPO). The chemical formula of L64 is $(PEO)_{13}(PPO)_{30}(PEO)_{13}$, having a mass of 2990 dalton. At low temperatures, both PEO and PPO are hydrophilic, and so L64 chains readily dissolve in water, existing as unimers. As the temperature increases, there is a decrease in the hydrogen-bond formation between water and polymer molecules, PPO tends to become less hydrophilic faster than PEO, and the copolymers acquire surfactant properties and aggregate to form micelles. Because at higher temperatures water progressively becomes a poor solvent to both PPO and PEO chains, the effective micelle-micelle interaction becomes attractive. The evidence for the increased short-range micellar attraction as a function of temperature comes from the existence of a critical point at $C = 0.05$ and $T = 330.9$ K and a percolation line (24–26). Theoretically, the phase behavior of the micellar system is characterized by an effective temperature $T^* = k_B T/u$, the volume fraction of the micelles ϕ, and the fractional attractive well width $\varepsilon = \Delta/d$, where k_B is the Boltzmann constant; $–u$, the depth of the attractive square well; Δ, the width of the well; and d, the diameter of the hard core.

The T-ϕ phase diagram of L64/D_2O system in the volume fraction range $0.520 < \phi < 0.550$ is shown in Fig. 1A. The dashed line depicts glass transition boundaries determined by three different experiments (22). The solid line gives the equilibrium phase boundary between the disordered micellar phase and the ordered liquid crystalline (hexagonal) phase (27). The amorphous states in the region of phase space under discussion are metastable states of the system, such as in supercooled liquids. In our system, crystallization does not happen unless the system is perturbed by an applied shear stress or placed very near a surface. Thus, the glass transition

Fig. 2. (A) The scaling plots of SANS intensities at $\phi = 0.535$ at different temperatures. Because the two-dimensional SANS pattern shows a single uniform ring, we conclude that the sample stays amorphous in the entire temperature range at this concentration. There are two distinct degrees of disorder (judging from the width of the peak), which depend on temperature. Whereas the narrower peak, which is resolution-limited, represents the glassy state, the broader peak, which is much broader than the resolution, represents the liquid state with a broader distribution of the interparticle distances. This figure indicates that the system shows a reentrant liquid–to–attractive glass–to–liquid transition. (B) The scaling plots of SANS intensities at $\phi = 0.542$ at different temperatures. A temperature-dependent degree of disorder characterizes the sys-

tem. Whereas the narrower peak is resolution limited, the slightly broader peak is also nearly resolution-limited but lower in intensity. It can be interpreted as showing a glass-to-glass transition (transition between two amorphous solid states with different degrees of disorder). The higher peak corresponds to the repulsive glass, and the lower peak, the attractive glass. (C) The scaling plots of SANS intensities at temperatures ranging from 293 to 325 K at $\phi = 0.544$, which is predicted to be the volume fraction in which the A_3 singularity point is located (see Fig. 1B). The two different types of glass become identical in their local structure at this volume fraction. (D) The scaling plots of SANS intensities at $\phi = 0.546$, a volume fraction beyond the A_3 point. Like (C), all the scaled intensities are again characterized by a unique length scale and collapse into one single master curve independent of temperature, showing identical local structure of the two glasses.

is observed in a metastable state of the micellar solution, which will last as long as we observe (for days). Figure 1B shows the the-oretical phase diagram in the T^*-ϕ plane, calculated by MCT with the use of an AHS for the specific case of $\varepsilon = 0.03$ (12). The solid line gives the liquid-to-glass phase boundaries, and the symbols represent part of the experimental data points mapped from Fig. 1A by analyzing small-angle neutron scattering (SANS) data taken in the liquid state (22). For this small value of ε, MCT predicts that there is a possibility of observing the transition between two distinct amorphous states within the volume fraction range from 0.536 to 0.544. Moreover, the glass-to-glass boundary terminates at A_3 [$\phi(A_3) = 0.544$], beyond which the long-time dynamics of two glassy states become identical.

In light of this knowledge, we made a series of SANS measurements on the micellar system within this volume fraction range to examine the local structure of the glassy states, especially at the A_3 point. In the amor-

phous states, a SANS intensity distribution, which reflects the local structure, is characterized by a single peak located at k_{max} or equivalently by a unique length scale $\Lambda = 1/k_{max}$, which is the mean distance between micelles. It is well known that SANS absolute intensity distribution of a two-phase system (the micelles and the solvent) is proportional to a three-dimensional Fourier transform of the Debye correlation function $\Gamma(r)$, and the Debye correlation function in this case must be of the form $\Gamma(r/\Lambda)$. Therefore, by a simple transformation of variables, the dimensionless, scaled intensity distribution can be put into a unique function of a scaled scattering wave vector y in the following form:

$$\frac{k_{max}^3 I(k)}{\langle \eta^2 \rangle} = \int_0^\infty dx\, 4\pi x^2 j_0(xy)\Gamma(x) \quad (1)$$

where $x = k_{max}r$, $y = k/k_{max}$, and $\langle \eta^2 \rangle$ is the so-called invariant of the scattering. Thus,

by plotting the scaled intensity as a function of scaled variable y, all the scattering intensity distributions at different temperatures within a single phase region should collapse into a single master curve. In this way, the distinct local structures associated with different phases occurring at different temperature ranges can be identified.

Four sets of the scaling plots as a function of temperature are shown in Fig. 2 at the four different volume fractions indicated in Fig. 1. At $\phi = 0.535$ (Fig. 2A), the transition between the ergodic (liquid) state and the nonergodic (attractive glass) state can be driven by varying the temperature in accord with the phase diagram shown in Fig. 1A. It shows a substantial difference between the local structure peaks of the resolution-limited nonergodic state and a much broader ergodic state peak. Furthermore, it should be noted that the transition shows a reentrant behavior (21, 22). By increasing ϕ to 0.542 (Fig. 2B), we drive the system into the phase region, where the two glass-forming mechanisms nearly balance each other ($T^* \sim$

Fig. 3. (**A**) The ISFs measured at $\phi = 0.535$, where the liquid–to–attractive glass transition is predicted, as a function of temperature. In the liquid state, the long-time limits of the ISFs, f_q values, are zero, whereas in the attractive glass state f_q is about 0.5, which is the DWF of the attractive glass state. The structural arrest transition is thus characterized by a discontinuous change of f_q called a bifurcation transition. The observed occurrence of a region of the logarithmic time dependence, preceding the plateau region for the system in the ergodic state just before the transition, is highlighted by a straight line in the linear-log plot. (**B**) The ISFs measured at $\phi = 0.542$. According to MCT, there is a possibility to observe glass-to-glass transition by varying T^*. Because $-u$ is temperature-dependent and increases on heating, T^* actually decreases as temperature rises, making the transition

from the repulsive glass region to the attractive glass region possible. By comparing the long-time limit of the ISFs with the predictions of MCT, we can identify the two different types of the glasses by the respective DWFs $f_q^A \sim 0.5$ and $f_q^R \sim 0.4$. The reason for observing two different values of DWFs can be interpreted as the different degrees of localization of density fluctuation in the two glasses. This figure combined with Fig. 2B give firm evidence of the repulsive glass ($f_q^R \sim 0.4$)–to–attractive glass ($f_q^A \sim 0.5$) transition. (**C**) The ISFs
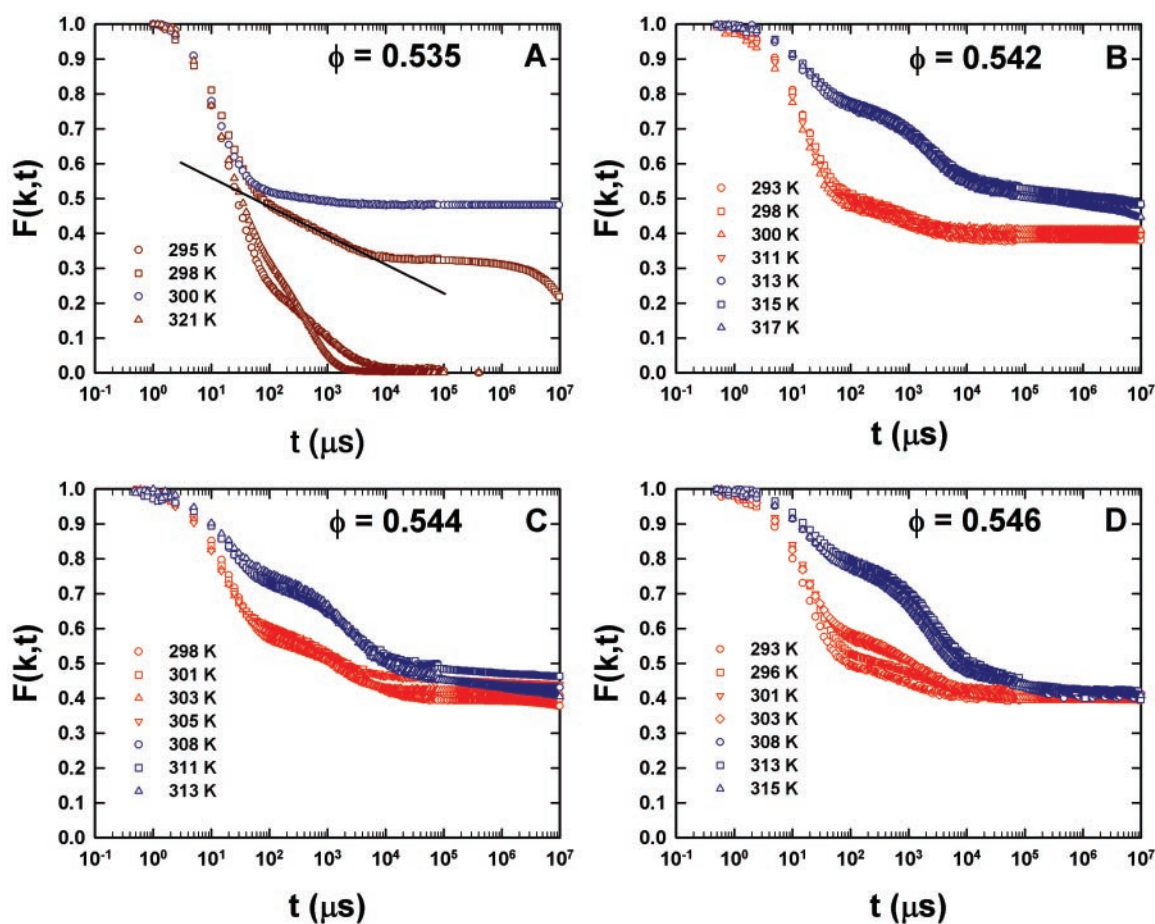
measured at $\phi = 0.544$, where, according to MCT, the long-time limit of ISF of the two glasses become identical. Our measured ISFs verify this prediction, showing an identical value of $f_q \sim 0.45$ for the two glassy states. Although the DWFs of these two types of glasses are identical, it is essential to recognize that there is a significant difference between the dynamics of their intermediate-time relaxations. (**D**) The ISFs measured at $\phi = 0.546$. This figure shares the same features as (C). It hints at critical point–like characteristics of the A_3 point.

1). Changing T in turn affects the well depth and thus T^*, and a transition from the repulsive glass (lower temperatures) to the attractive glass (higher temperatures) is triggered. In Fig. 2B, we see two distinct sets of resolution-limited peaks, with the one for the repulsive glass higher than the one for the attractive glass. Thus, we can conclude that the repulsive glass is better ordered locally than the attractive glass. At $\phi = 0.544$ (Fig. 2C, the A_3 point), we see that the two sharp peaks merge into one sharp peak independent of temperature, signifying that the local structures of the two glasses become identical. Increasing ϕ further to 0.546 (Fig. 2D), the situation remains the same as in the previous volume fraction. This is proof that the MCT predictions are accurate.

Photon correlation spectroscopy was used to investigate the predicted dynamical singularity at the A_3 point. In Fig. 3, intermediate scattering functions (ISFs) measured at $k = 0.00222$ Å^{-1} and at the same four different volume fractions as before are shown as a function of temperature. In Fig. 3A, the ISF measured in an ergodic state exhibits a logarithmic relaxation (indicated by a straight-line fit) at intermediate times followed by a power-law decay before the final α relaxation, in agreement with MCT. The nonergodic state ($T = 300$ K), which has a finite plateau at long times as indicated by the ISF, represents the attractive glass for which the Debye-Waller factor (DWF, the height of the plateau) is about 0.5. Upon increasing ϕ to 0.542 (Fig. 3B), we see that all the ISFs can be grouped into two distinct sets of curves having two different values of DWF: one at 0.5 (attractive glass) and the other at 0.4 (repulsive glass). ISFs in Fig. 3, C and D, indicate that at A_3 and beyond, the DWF of the two glassy states become identical. This is proof of the existence of the A_3 singularity in the phase diagram occurring at exactly the predicted volume fraction. It is, however, worth noting that at A_3 and beyond, the intermediate-time relaxations (the β relaxation region) of the two glassy states are clearly different in spite of the fact that the long-time relaxation becomes identical.

We used photon correlation spectroscopy to verify that the L64/D$_2$O micellar system follows the phase behavior predicted by MCT with the use of a square well potential with a short-range attraction ($\varepsilon = 0.03$). In particular, we show experimentally the existence of the A_3 singularity in the predicted phase diagram. Our SANS experiment further shows that although the local structures of the attractive and repulsive glasses are in general different, they become identical at the A_3 singularity. It is intriguing to speculate the extent to which one can draw the analogy between the A_3 singularity and the ordinary equilibrium critical point.

References and Notes

1. W. B. Russel, *Colloidal Dispersions* (Cambridge Univ. Press, London, 1992).
2. W. Götze, in *Liquids, Freezing and the Glass Transition*, J. P. Hansen, D. Levesque, J. Zinn-Justin, Eds. (North-Holland, Amsterdam, 1991), part I, pp. 287–503.
3. W. Götze, L. Sjögren, *Rep. Prog. Phys.* **55**, 241 (1992).
4. P. N. Pusey, W. van Megan, *Phys. Rev. Lett.* **59**, 2083 (1987).
5. W. van Megan, P. N. Pusey, *Phys. Rev. A* **43**, 5429 (1991).
6. W. van Megan, S. M. Underwood, *Phys. Rev. E* **49**, 4206 (1994).
7. E. R. Weeks, J. C. Crocker, A. C. Levitt, A. Schofield, D. A. Weitz, *Science* **287**, 627 (2000).
8. E. R. Weeks, D. A. Weitz, *Phys. Rev. Lett.* **89**, 095704 (2002).
9. M. Fuchs, *Transp. Theory Stat. Phys.* **24**, 855 (1995).
10. E. Bartsch, M. Antonietti, W. Schupp, H. Sillescu, *J. Chem. Phys.* **97**, 3950 (1992).
11. T. Eckert, E. Bartsch, *Phys. Rev. Lett.* **89**, 125701 (2002).
12. K. Dawson *et al.*, *Phys. Rev. E* **63**, 011401 (2001).
13. E. Zaccarelli, G. Foffi, K. A. Dawson, F. Sciortino, P. Tartaglia, *Phys. Rev. E* **63**, 031501 (2001).
14. L. Fabbian, W. Götze, F. Sciortino, P. Tartaglia, F. Thiery, *Phys. Rev. E* **59**, R1347 (1999).
15. J. Bergenholtz, M. Fuchs, *Phys. Rev. E* **59**, 5706 (1999).
16. ———, *J. Phys. Condens. Matter* **11**, 10171 (1999).
17. E. Bartsch, T. Eckert, C. Pies, H. Sillescu, *J. Non-Cryst. Solids* **307–310**, 802 (2002).
18. K. N. Pham *et al.*, *Science* **296**, 104 (2002).
19. F. Mallamace *et al.*, *Phys. Rev. Lett.* **84**, 5431 (2000).
20. P. N. Segrè, V. Prasad, A. B. Schofield, D. A. Weitz, *Phys. Rev. Lett.* **86**, 6042 (2001).
21. In a recent study (*28*), we found that within a certain volume fraction range, a reentrant transition from liquid (L) to attractive glass (AG) to liquid to repulsive glass (RG) (i.e., L-AG-L-RG) is observed upon increasing the temperature from 283 to 343 K.
22. W. R. Chen, S. H. Chen, F. Mallamace, *Phys. Rev. E* **66**, 021403 (2002).
23. For example, see E. G. Ponyatovsky, O. I. Barkalov, *Mater. Sci. Rep.* **8**, 147 (1992).
24. S. H. Chen, C. Liao, E. Fratini, P. Baglioni, F. Mallamace, *Colloids Surf. A* **95**, 183 (1999).
25. C. Y. Liao, S. M. Choi, F. Mallamace, S. H. Chen, *J. Appl. Crystallogr.* **33**, 677 (2000).
26. L. Lobry, N. Micali, F. Mallamace, C. Liao, S. H. Chen, *Phys. Rev. E* **60**, 7076 (1999).
27. K. W. Zhang, B. Lindman, L. Coppola, *Langmuir* **11**, 538 (1995).
28. W. R. Chen, S. H. Chen, F. Mallamace, in preparation.
29. The research at MIT is supported by a grant from Materials Science Division of U.S. DOE. The research in Messina is supported by INFM-PRA98 and MURST-PRIN2000. We are grateful to C. Glinka of the Center of Neutron Research (National Institute of Standards and Technology) and P. Thiyagarajan of the Intense Pulsed Neutron Source (Argonne National Laboratory) for the beam time of NG7 and SAND spectrometers, respectively, and for their technical assistances.

14 January 2003; accepted 24 March 2003

All-Metal Antiaromatic Molecule: Rectangular Al₄⁴⁻ in the Li₃Al₄⁻ Anion

Aleksey E. Kuznetsov,[1] K. Alexander Birch,[1] Alexander I. Boldyrev,[1]* Xi Li,[2,3] Hua-Jin Zhai,[2,3] Lai-Sheng Wang[2,3]*

We report the experimental and theoretical characterization of antiaromaticity in an all-metal system, Li$_3$Al$_4^-$, which we produced by laser vaporization and studied with the use of photoelectron spectroscopy and ab initio calculations. The most stable structure of Li$_3$Al$_4^-$ found theoretically contained a rectangular Al$_4^{4-}$ tetraanion stabilized by the three Li$^+$ ions in a capped octahedral arrangement. Molecular orbital analyses reveal that the rectangular Al$_4^{4-}$ tetraanion has four π electrons, consistent with the $4n$ Hückel rule for antiaromaticity.

The stabilization of aromatic systems (*1*), cyclic systems with $4n + 2$ π electrons, was first understood in organic molecules. On the basis of these ideas, numerous inorganic aromatic molecules have been synthesized and characterized, including all-metal systems (*2–7*). The concept of antiaromaticity, the corresponding destabilization seen in cyclic systems with $4n$ π electrons, was introduced by Breslow (*8, 9*) and is perhaps best understood in cyclobutadiene. However, examples of antiaromatic compounds outside of organic chemistry do not appear to have been reported.

We explored whether an antiaromatic all-metallic compound could be synthesized on the basis of an all-metal aromatic system, Al$_4^{2-}$ (*3*). This molecule, which is stabilized by a counterion such as Li$^+$, contains two π electrons and assumes a square shape. The reduced species, Al$_4^{4-}$, would contain four π electrons and would take on a rectangular shape if the two additional electrons entered a π orbital.

We used a laser vaporization source to make such a species stabilized by Li$^+$ in the form of Li$_3$Al$_4^-$, and then studied it with anion photoelectron spectroscopy (*10–12*). We made the Li$_3$Al$_4^-$ clusters with an Al-Li

[1]Department of Chemistry and Biochemistry, Utah State University, Logan, UT 84322, USA. [2]Department of Physics, Washington State University, 2710 University Drive, Richland, WA 99352, USA. [3]W. R. Wiley Environmental Molecular Sciences Laboratory, Pacific Northwest National Laboratory, Mail Stop K8-88, Post Office Box 999, Richland, WA 99352, USA.

*To whom correspondence should be addressed. E-mail: boldyrev@cc.usu.edu, ls.wang@pnl.gov